

FDRN: A Fast Deformable Registration Network for Medical Images

Kaicong Sun*, Sven Simon

Institute of Parallel and Distributed Systems, University of Stuttgart, Stuttgart, Germany

*Corresponding author. Email: kaicong.sun@ipvs.uni-stuttgart.de

Abstract

Purpose: Deformable image registration is a fundamental task in medical imaging. Due to the large computational complexity of deformable registration of volumetric images, conventional iterative methods usually face the tradeoff between the registration accuracy and the computation time in practice. In order to boost the performance of deformable registration in both accuracy and runtime, we propose a fast unsupervised convolutional neural network for deformable image registration.

Methods: The proposed FDRN possesses a compact encoder-decoder structure which employs a pair of fixed and moving images as input and outputs a three-channel displacement vector field (DVF) describing the offsets between the corresponding voxels in the fixed and moving images. The model is trained in an unsupervised fashion by optimizing a loss function which punishes the dissimilarity between the fixed and the transformed moving images. Specially, deep supervision is achieved by integrating an auxiliary loss acting on the bottom low-resolution feature maps. Additive forwarding which couples the encoder path with the corresponding decoder counterpart is deployed to propagate the fine structures efficiently without consuming extra memory. Besides, skip connection adopted at each encoder and decoder stage enables residual learning and improves the learning efficiency. A 3D total variation (TV) is incorporated into the loss function as regularization to constrain the smoothness of DVF.

Results: We conducted experiments on the LPBA40 brain MRI dataset which contains 40 subjects with the segmentation labels for 56 structures including the hippocampi. A comparison with the existing state-of-the-art approaches was carried out. The experimental results demonstrate that our FDRN performs better than the other methods qualitatively and quantitatively in Dice score and normalized cross correlation (NCC). In addition, we evaluated the generalizability of FDRN by performing registration on 20 randomly selected samples from the unseen ABIDE and ADNI MRI datasets. The proposed FDRN shows desirable generalizability and robustness against unseen data and provides promising performance in NCC and visual perception.

Conclusions: The proposed FDRN provides better performance than the existing state-of-the-art registration methods for brain MR images by resorting to the compact autoencoder structure and deep supervision. Besides, FDRN is a generalized framework which is not confined to a particular type of medical images or anatomy. It can also be applied to other anatomical structures or CT images.

Keywords: Deformable image registration, unsupervised learning, deep supervision, human brain MRI registration, encoder-decoder network, auxiliary loss

I. Introduction

Deformable medical image registration is an approach to establish dense spatial correspondence between a pair of digital images based on the local morphological structures. Deformable registration is widely applied to many medical applications such as detecting temporal anatomical changes of individuals, analyzing variability across populations, and multi-modality fusion. In last decades, fruitful achievements have been obtained^{1–4}. Most of the existing conventional algorithms optimize an objective function which consists of a data fidelity term D and a regularization term R formulated as following:

$$J = -D(F(\mathbf{x}), \phi \circ M(\mathbf{x})) + \lambda R(\phi). \quad (1)$$

The data fidelity term D measures the alignment between the fixed image F and the transformed moving image $\phi \circ M$ with ϕ being the dense deformation field which maps the coordinates of F to the coordinates of M . \mathbf{x} denotes the 3D spatial coordinate in domain $\{\Omega \mid \Omega \subset \mathbb{R}^3\}$. The most commonly used data terms are based on, e.g., L_2 error norm⁵, mutual information⁶, and cross-correlation⁷. As deformable registration is a highly ill-posed problem, regularization R is inevitably required to encode the prior knowledge of the transformation such as smoothness into the objective function. The weighting parameter λ balances the tradeoff between the data term D and the regularization term R . The deformation field ϕ is usually formulated as $\phi = \mathbf{x} + d(\mathbf{x})$ with $d(\mathbf{x})$ being the displacement vector field (DVF) which represents the spatial offsets between the corresponding voxels in the fixed and the moving images. Particularly,^{8–10} estimate the deformation based on the linear elastic models. In^{11–13}, the deformation field is described by cubic B-spline. A diffusion model Demons is introduced by Thirion for deformable registration in¹⁴. Generally, the DVF-based models can not guarantee an inverse consistency such that interchanging the order of the two input images, the obtained transformation may not match the inverse of the counterpart. Different to the DVF-based deformation field, diffeomorphic registration describes the deformation as an integral of a velocity vector field which possesses biomedical properties such as diffeomorphism, topology preservation, inverse consistency, and symmetry^{5,7,15,16}. The Large Diffeomorphic Distance Metric Mapping (LDDMM) presented by Beg *et al.*⁵ solves a global variational problem in the space of smooth velocity vector field. Avants *et al.*⁷ propose the symmetric normalization method (SyN) using cross-correlation as the similarity measure. However, due to the huge computational demand for volumetric medical images, tackling practical problems by conventional methods could be extremely slow.

In contrast to the traditional optimization-based methods which adopt iterative updating scheme, learning-based methods are usually trained offline based on a large-scale dataset. As long as the parameters of the models are well-trained, predicting the transformation between unseen images performs solely forward propagation and consumes significantly less computation time. In other words, the learning-based methods transfer the burdens of computation to offline training and the well-trained model is dedicated to the specific application covered in the training dataset. Abundant learning-based studies on medical image registration have been conducted in the last two decades^{17–23}. In particular, Kim *et al.*²² present a patch-based deformation model using sparse representation. In²¹, Gutiérrez-Becker *et al.* formulate the prediction of the transformation parameters as supervised regression using the

gradient boosted trees.^{24–27} adopt deep convolutional neural network (CNN) in a supervised manner for taking advantage of the outstanding feature extraction ability. More recently, some works^{28–30} propose CNN models based on unsupervised learning by optimizing the similarity match between the fixed image and the transformed moving image resorting to the spatial transformer network (STN)³¹. Specially, Balakrishnan *et al.*²⁹ introduce a CNN framework based on the UNet structure³² adopting local cross-correlation as the data fidelity term. In³⁰, Li *et al.* construct a multi-resolution registration model which contains three losses constraining the DVF at different spatial resolutions. In³³, the authors extend their previous work²⁹ by introducing Dice scores of the segmented regions as the regularization. In contrast to²⁹, we propose a compact deep CNN model based on the autoencoder structure adopting additive forwarding, skip connection and deep supervision. The proposed FDRN achieves better performance than the existing state-of-the-art registration performance for brain MR images. Besides, FDRN is a generalized registration model and is not limited to a particular type of image or anatomic structure.

The paper is organized as follows. In Section II., we introduce the proposed FDRN model for deformable registration. Section III. demonstrates the experimental results quantitatively and qualitatively on different MRI datasets. We discuss the insights of the experiments and conclude in Section IV..

II. Materials and Methods

The proposed FDRN is based on a compact encoder-decoder structure as demonstrated in Fig. 1. FDRN has a two-channel input which consists of a fixed and moving image pair and outputs a three-channel displacement vector field (DVF) which describes the offsets between the corresponding voxels in the fixed and moving images. Based on the resultant DVF $d(\mathbf{x})$, the moving image M is resampled at the transformed nonvoxel locations $\phi(\mathbf{x}) = \mathbf{x} + d(\mathbf{x})$ and a similarity measure between the fixed image F and the transformed moving image $\phi \circ M$ can be optimized. Hence, the model can be trained in an unsupervised scheme regardless of the ground-truth DVF. Particularly, the encoder path extracts the features at different resolutions and meanwhile enlarges the receptive field by downscaling the feature maps. Skip connection is utilized at each encoder and decoder stage to enable residual learning. Besides, an auxiliary loss is involved at the bottom layer of the encoder path to deeply supervise the learning of the model. Actually, the bottom layer is upsampled and acts as a DVF in the lower resolution grid. On the decoder side, the extracted features are fused and the feature maps are enlarged to restore the original image dimension. Aiming for saving memory and runtime, instead of using concatenation as VoxelMorph²⁹, we adopt additive forwarding to propagate structural details from the encoder path to the corresponding decoder counterpart. Combining the auxiliary loss with the main loss which is performed on the full resolution, we yield the overall loss formulated as below:

$$L_{overall} = (1 - \lambda)L_{main} + \lambda L_{aux}. \quad (2)$$

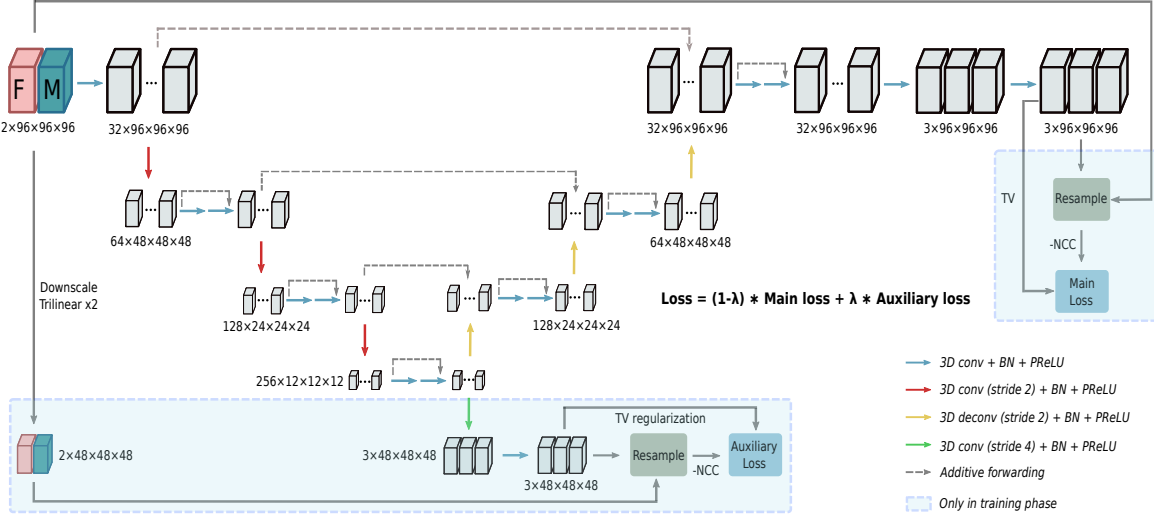


Figure 1: Schematic illustration of the structure of the proposed FDRN.

The parameter $\lambda \in [0, 1]$ is dedicated to balancing the main loss L_{main} and the auxiliary loss L_{aux} . In particular, L_{main} and L_{aux} are defined as

$$\begin{aligned} L_{main} &= -D(F_h(\mathbf{x}), \phi_h \circ M_h(\mathbf{x})) + \alpha_1 R(\phi_h), \\ L_{aux} &= -D(F_l(\mathbf{x}), \phi_l \circ M_l(\mathbf{x})) + \alpha_2 R(\phi_l), \end{aligned} \quad (3)$$

where D denotes the data fidelity term and we adopt normalized cross-correlation (NCC) as expressed in Eq. (4) to quantify the similarity measure. ϕ_h and ϕ_l indicate respectively the deformation field at the high and low resolutions. A 3D total variation (TV) formulated in Eq. (5) serves as the regularization to impose the smoothness constrain on the DVF. α_1, α_2 are the weights for the TV regularization.

$$D(F, \phi \circ M) = \frac{\sum_{\mathbf{x}}^{\Omega} (F(\mathbf{x}) - \bar{F})(\phi \circ M(\mathbf{x}) - \overline{\phi \circ M})}{N \sqrt{\text{var}(F(\mathbf{x})) \text{var}(\phi \circ M(\mathbf{x}))}} \quad (4)$$

In the formulation of NCC in Eq. (4), \bar{F} indicates the mean of the fixed image and $\overline{\phi \circ M}$ represents the mean of the transformed moving image. N denotes the overall amount of voxels in the fixed or moving image and $\text{var}(\cdot)$ represents the variance operator.

As the deformation field ϕ is a linear combination of the identity transform \mathbf{x} and the expected DVF, we apply 3D TV constraint directly on the DVF $d(\mathbf{x})$:

$$R(d(\mathbf{x})) = \sum_{S_k} \|d(\mathbf{x}) - S_k d(\mathbf{x})\|_1, \quad (5)$$

where S_k indicates the shifting operator along (u, v, w) direction by vector k with $k = \{(u, v, w) \mid u, v, w \in \{0, 1\}\}$ and $\|\cdot\|_1$ represents the L1-norm.

The transformation of the moving image $\phi \circ M(\mathbf{x})$ can be implemented by a trilinear interpolation of $M(\mathbf{x})$ at the nonvoxel locations ϕ . Specially, the resampling of $M(\mathbf{x})$ at the

transformed location ϕ is formulated as

$$\phi \circ M(\mathbf{x}) = \sum_{\mathbf{n} \in \mathbf{N}(\phi(\mathbf{x}))} M(\mathbf{n}) \prod_{m \in \{u,v,w\}} (1 - |\phi_m(\mathbf{x}) - \mathbf{n}_m|), \quad (6)$$

where $\mathbf{N}(\phi(\mathbf{x}))$ denotes the neighbors of the transformed location in the moving image $M(\mathbf{x})$ and \mathbf{n} represents the coordinates of the individual neighbor. m is an indicator and iterates over the dimensions of the moving image.

III. Results

In this section, we conducted experiments to evaluate the proposed FDRN from different aspects. Particularly, in Section III.D. we trained and tested FDRN on the LONI LPBA40 dataset³⁴ which contains T1-weighted brain MR images of 40 neurologically intact nonepileptic subjects with expert segmentation of 56 regions. We compared FDRN with the state-of-the-art learning-based methods Li *et al.*³⁰, VoxelMorph²⁹ and the traditional method symmetric image normalization SyN⁷. In Section III.E., we validated the well-trained FDRN on a collection of the unseen samples from ABIDE³⁵ and ADNI³⁶ MRI datasets. Section III.F. contains the ablation study of FDRN and the experimental analysis on the weighting parameter of the auxiliary loss and the weight of the TV regularization.

III.A. Datasets and Preprocessing

The LPBA40 dataset contains 40 MR images with segmentation labels for 56 brain regions including the hippocampi. All of these MR images were firstly registered to the Montreal Neurological Institute (MNI) space using affine transformation based on the ICBM152 template³⁷ as preprocessing. The registered images were then cropped to the size of $160 \times 208 \times 176$. We partitioned the 40 cropped images into 30 and 10 for training and testing accordingly. In addition, we selected 10 images respectively from the preprocessed ABIDE³⁵ and ADNI³⁶ MRI datasets to evaluate the generalizability of the proposed FDRN. The experimental results are demonstrated in Section III.D. and Section III.E..

III.B. Evaluation Metrics

In addition to NCC which measures the similarity match, we evaluate the registration performance using Dice score³⁸ to quantify the overlap of labels for each segmented region in percentage which is formulated as following:

$$Dice(A, B) = \frac{2 * |A \cap B|_1}{|A|_1 + |B|_1}, \quad (7)$$

where A and B indicate binary images which represent the individual label in the fixed and moving image, respectively. Furthermore, we leverage the perception-based metric,

structural similarity index measure (SSIM)³⁹, to aid the assessment in visual perception in terms of luminance, contrast and structure:

$$SSIM(A, B) = \frac{(2\mu_A\mu_B + c_1)(2\sigma_{AB} + c_2)}{(\mu_A^2 + \mu_B^2 + c_1)(\sigma_A^2 + \sigma_B^2 + c_2)}, \quad (8)$$

where $\mu_A, \mu_B, \sigma_A, \sigma_B$ denote the mean and standard deviation of the image A and B . σ_{AB} indicates the covariance between image A and B . c_1, c_2 are constants to stabilize the division with weak denominator. An SSIM of 1 indicates a perfect anatomical match.

III.C. Implementation of Baseline Model and FDRN

We implemented the FDRN with a Pytorch backend. A baseline model has a lightweight structure which contains a single convolutional layer at each encoder and decoder stage and the amount of channels is reduced to 24, 48, 96, 192. Extended from the baseline model, FDRN has two convolutions at each stage and 32, 64, 128, 256 channels to deepen the network and enlarge the model capacity. During the training phase, a mini-batch of size 2 was used and the patch size was set as $96 \times 96 \times 96$. We employed ADAM as the optimizer and the learning rate was chosen as 0.001 over 10 epochs. The weight λ of the auxiliary loss was selected as 0.3 and the weighting parameters α_1, α_2 for TV regularizations were set as $\alpha_1 = 10^{-8}, \alpha_2 = 8\alpha_1$. The experiments were performed on the NVIDIA GeForce GTX 1080 Ti GPU and Intel(R) Xeon(R) E5-2650 v2 CPU.

III.D. Evaluation on LPBA40 Dataset

We conducted comparison with the existing state-of-the-art deformable registration methods SyN⁷, Li *et al.*³⁰ and VoxelMorph²⁹ on the public LPBA40 dataset. Specially, we reproduced and trained Li's model, VoxelMorph in Pytorch and employed ANTsPy, the Python wrapper for the Advanced Normalization Tools (ANTs)⁴⁰, to implement SyN. We doubled the amount of feature channels of VoxelMorph as proposed in³³ to account for the increased inherent variability for the subject-to-subject registration. 30 preprocessed MR images were used as the training data and the remaining 10 images constructed the testing data. Every two out of the 30 images were selected as the input during the training phase. In the testing phase, each of the 10 images was chosen as the fixed image and the rest 9 images were registered to it. Hence, during the testing phase we carried out registration for 90 pairs of images. We quantified the performance of SyN, Li's method, VoxelMorph, our baseline model and FDRN using Dice score, NCC and runtime as depicted in Tab. 1. As depicted, all of the CNN-based methods perform better in NCC than the traditional SyN. Particularly, Li's method and VoxelMorph achieve comparable Dice score as SyN. Comparing to VoxelMorph, our baseline model obtains a performance gain of 0.48% in Dice. The proposed FDRN improves the Dice and NCC further by enlarging the network capacity. Besides, the learning-based methods complete image registration within one second on the GPU. To our knowledge, ANTs does not have a GPU implementation. Comparing the computation time on a CPU, SyN requires

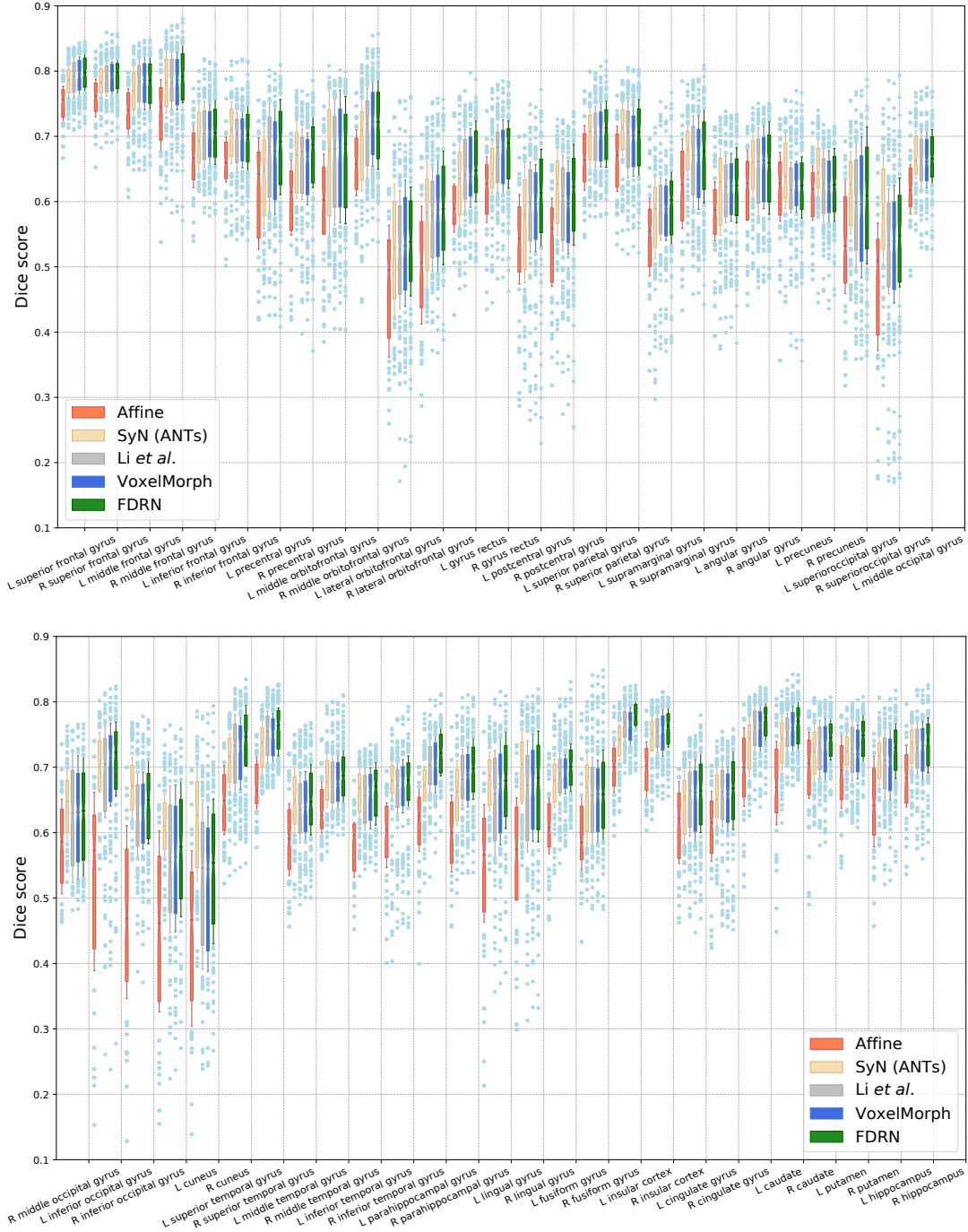


Figure 2: Boxplots of the Dice scores of 54 labeled anatomical regions for the 90 testing image pairs from the publicly available LPBA40 brain MRI dataset. Affine represents the results of the globally registered images based on affine transformation in the preprocessing step. SyN indicates the results by the traditional symmetric image normalization method which was implemented by ANTsPy. Li *et al.* and VoxelMorph are the learning-based state-of-the-art registration methods. It is shown that the proposed FDRN performs best in Dice score for most of the regions.

Table 1: Comparison of different registration methods on the testing images with size of $160 \times 208 \times 176$ in the LPBA40 MRI dataset by average Dice score, NCC and runtime.

	Affine	SyN ⁴⁰	Li <i>et al.</i> ³⁰	VoxelMorph ²⁹	Our baseline	FDRN
Dice	0.6084	0.6699	0.6652	0.6664	0.6712	0.6750
NCC	0.9504	0.9817	0.9945	0.9962	0.9963	0.9973
Time (GPU)	–	–	0.37s	0.45s	0.65s	1.00s
Time (CPU)	–	1385.25s ^a	71.06s	208.39s	189.21s	338.83s

^a SyN was conducted by ANTsPy and executed on the Intel(R) Xeon(R) E5-2650 v2 CPU.

1385.25s to achieve comparable Dice score, while our baseline model consumes 189.21s. It is worth noting that the runtime is accumulated purely for the registration step without concerning the preprocessing and image loading. In addition, we present the Dice score of each anatomical structure labeled in LPBA40 by different methods in the boxplots shown in Fig. 2. We can observe that FDRN performs best for most of the labeled regions.

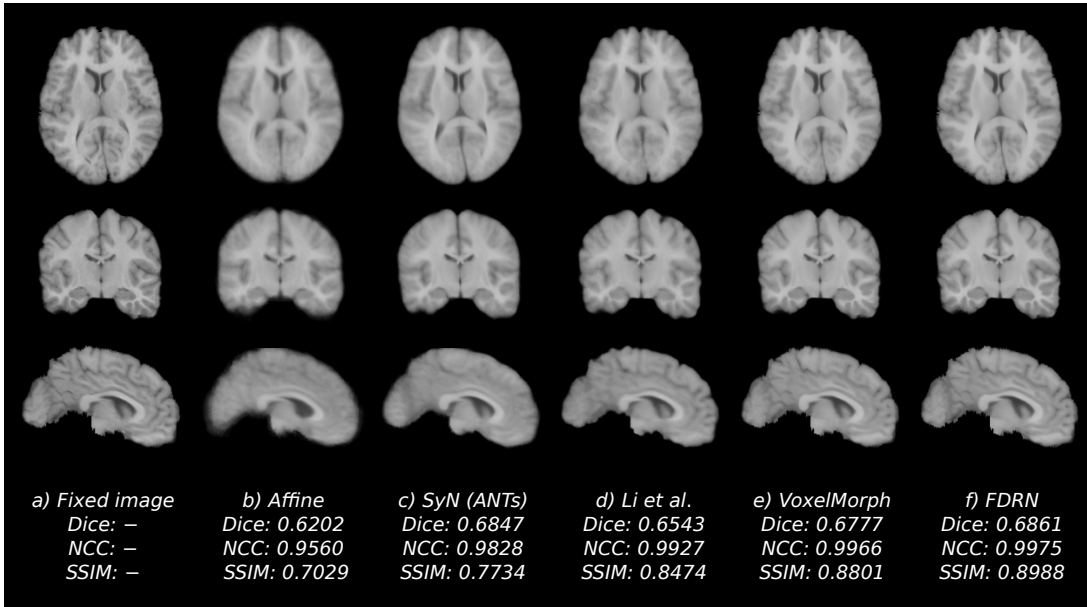


Figure 3: Visual evaluation of different registration methods on LPBA40 MRI dataset. One of the 10 testing images was chosen as the fixed image and the rest 9 images were registered to it. The average of the 9 registered images is illustrated. The mean of Dice score, NCC and SSIM by individual method are presented underneath.

In order to evaluate FDRN visually, we selected one image from the 10 testing images in LPBA40 as the fixed image and registered the remaining 9 images to it. We demonstrate the average of the 9 registered images in different views and present the mean of Dice score, NCC and SSIM of different methods in Fig. 3. It is shown that the average images of affine and SyN are severely blurred, while FDRN provides a sharper and more desirable result. Besides, FDRN provides the best NCC and SSIM which coincides with the visual perception.

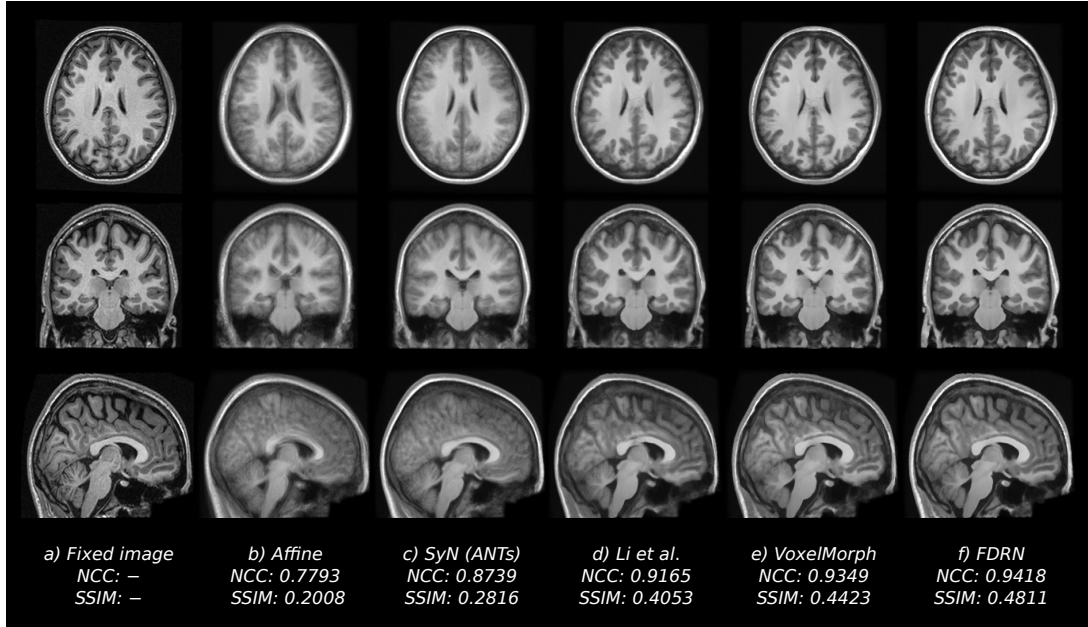


Figure 4: Visual evaluation of the well-trained models on 10 randomly selected images from the unseen ABIDE MRI dataset. One of the 10 images was utilized as the fixed image and the rest 9 images were registered to it. The average of the 9 registered images is illustrated with the corresponding mean of NCC and SSIM.

III.E. Evaluation on ABIDE and ADNI Datasets

We evaluated the generalizability of the proposed FDRN by performing registration on 20 randomly selected images from the unseen ABIDE and ADNI MRI datasets without retraining. Due to the lack of segmentation labels, we assessed the registration performance by NCC and SSIM. Specially, we randomly selected 10 images out of each dataset. One image was chosen as the fixed image and the remaining 9 images were registered to it. The average of the 9 registered images in ABIDE and in ADNI by different methods are shown in Fig. 4 and Fig. 5, respectively. The sharpness of the average registered images indicates the generalizability and robustness of the models. As we can see, the well-trained FDRN performs best on the unseen images quantitatively in NCC and SSIM and also qualitatively in visual perception. Li’s method seems lack of generalizability for the unseen data due to the shallow structure. SyN may need more computational effort for registering images with large variation.

III.F. Ablation Study and Parameter Analysis

We present the ablation study of the proposed FDRN with regard to the auxiliary loss, additive forwarding which links the encoder path to the decoder counterpart and the skip connection adopted at each encoder and decoder stage. The experiment was performed on the LPBA40 dataset and evaluated by the Dice score and NCC as depicted in Tab. 2. It is

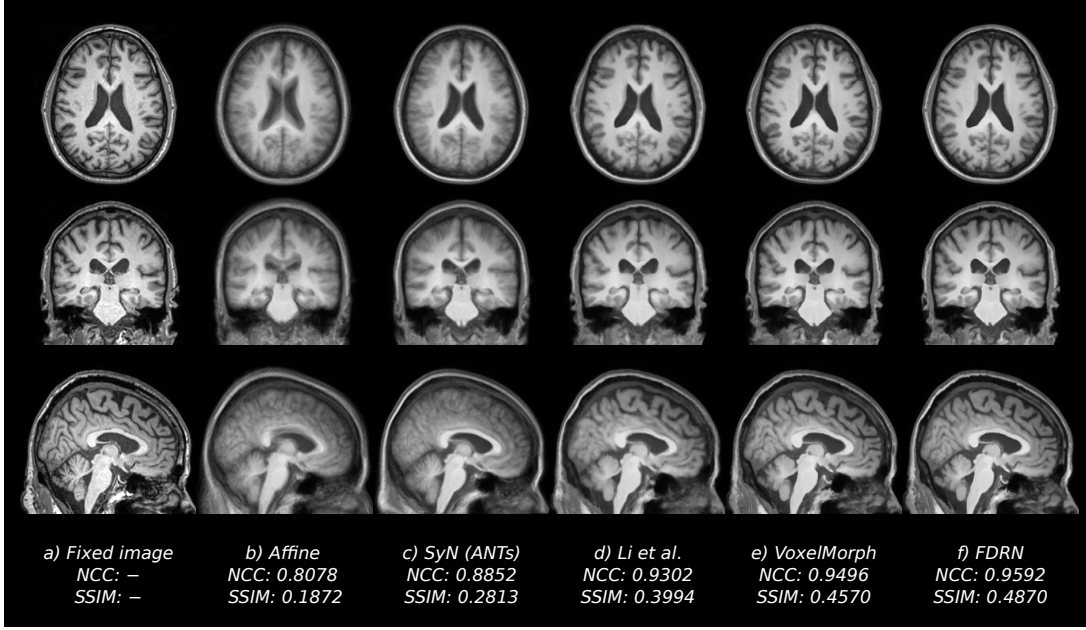


Figure 5: Visual evaluation of the well-trained models on 10 randomly selected images from the unseen ADNI MRI dataset. One of the 10 images was utilized as the fixed image and the rest 9 images were registered to it. The average of the 9 registered images is illustrated with the corresponding mean of NCC and SSIM.

interesting to show that the Dice score and NCC are not always consistent with each other. Specially, as we can observe that additive forwarding improves the NCC but may complicate the labeling. On the contrary, auxiliary loss contributes mainly to Dice score by exploiting the spatial correspondence in the low-resolution grid. The skip connection benefits both the Dice and NCC by residual learning. Furthermore, we can observe that without utilizing the auxiliary loss degrades the performance in Dice severely. Employing all of them in the model improves the Dice by 1% and the NCC by 0.0023.

Additionally, we analyzed the impact of the weighting parameter of the auxiliary loss λ and the weight of the regularization term α_1 on the Dice score. Fig. 6 a) exhibits the average Dice of FDRN with varied λ on the LPBA40 dataset. Empirical results show that $\lambda = 0.3$ improves the performance in Dice score most. In Fig. 6 b), it is shown that $\alpha_1 = 10^{-8}$ provides the best Dice score and aggressive TV regularization deteriorates the Dice dramatically.

Table 2: Ablation study of the proposed FDRN based on Dice score and NCC on the LPBA40 dataset.

Add. forward.	✗	✓	✗	✗	✓	✓	✗	✓
Skip connect.	✗	✗	✓	✗	✓	✗	✓	✓
Auxiliary loss	✗	✗	✗	✓	✗	✓	✓	✓
Dice	0.6632	0.6563	0.6669	0.6644	0.6623	0.6690	0.6696	0.6732
NCC	0.9943	0.9952	0.9955	0.9945	0.9964	0.9959	0.9959	0.9966

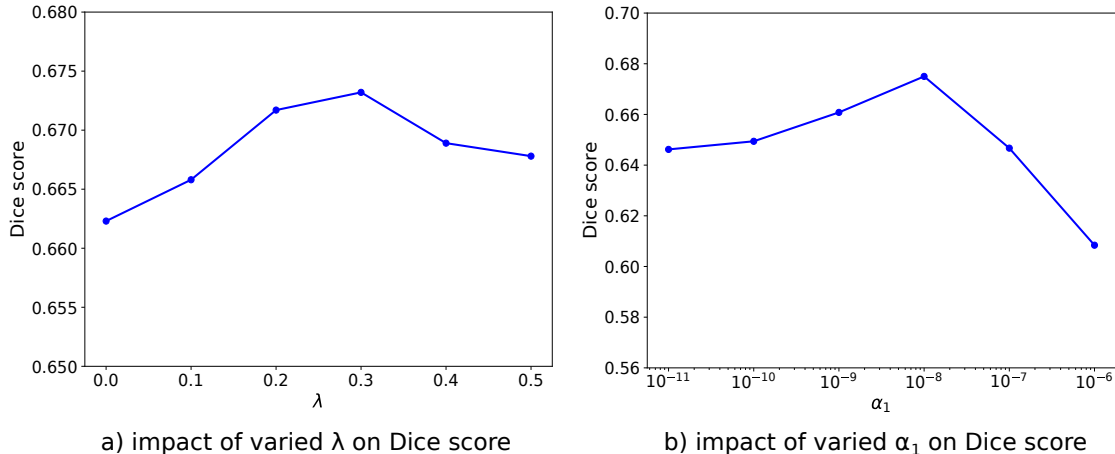


Figure 6: Dice score of FDRN on the LPBA40 dataset with a) varied regularization weight of the auxiliary loss λ ; b) varied weight of the TV regularization α_1 .

IV. Discussion and Conclusion

The proposed fast deformable registration network FDRN achieves better performance in Dice score, NCC and visual perception than the existing state-of-the-art methods for deformable registration of MR images of human brains. Specially, we trained and evaluated FDRN on the publicly available LPBA40 MRI dataset. A comparison with other existing state-of-the-art registration methods has been conducted including the well-known symmetric image normalization (SyN), Li’s method, and VoxelMorph. We adopted Dice score and NCC as the evaluation metrics. Comparing to VoxelMorph, our baseline model performs better in Dice score by 0.48%. FDRN further improves the registration performance by enlarging the model capacity and obtains a performance gain of 0.86% in Dice. For visual comparison, we involved the perception-based metric SSIM to aid the assessment. Experiments show that the average of the registered images by FDRN obtains sharper anatomical structures than the other methods which indicates that FDRN has better registration accuracy and strong robustness against different variants of the moving image. Although SyN provides comparable Dice score as FDRN, the visual quality is less satisfactory and the average image is fairly blurred which coincides with the NCC and SSIM.

In order to explore the generalizability of the FDRN, we performed registration on 20 randomly selected images from the unseen ABIDE and ADNI MRI datasets. Due to the lack of the segmentation labels, we assessed the performance visually and quantitatively by NCC and SSIM. It is shown that the proposed FDRN has the best NCC and SSIM among all the investigated methods. Specially, FDRN obtains a performance gain of 0.0069 and 0.0096 in NCC respectively on ABDIE and ADNI datasets compared to VoxelMorph. Besides, FDRN generates obviously sharper and desirable results in visual perception. By resorting to the compact model structure and efficient learning, FDRN provides robust registration and achieves promising generalizability for the unseen images of inherent variability.

In the ablation study, we explored the contribution of different components of the model

to the performance improvement. Specially, we analyzed the impact of the auxiliary loss, additive forwarding and skip connection on the Dice score and NCC. Empirical results demonstrate that the auxiliary loss benefits the network mainly in Dice and the weight of the auxiliary loss at 0.3 leads to the best Dice score. The additive forwarding improves mainly the NCC by propagating the structural details from the encoder path straightly to the decoder path and refining the localization accuracy. The skip connection contributes to the Dice and NCC simultaneously by improving the learning efficiency using residual learning.

With regard to computation time, the learning-based methods accomplish deformable registration of images of size $160 \times 208 \times 176$ within one second on the GPU. Due to the lack of the GPU implementation of the traditional method SyN in the software package ANTs, we compared the runtime on the CPU. SyN requires averagely 1385.25s to achieve comparable Dice score as our baseline model, while the baseline model consumes only 189.21s. Regardless of the Dice score, the baseline model performs better than SyN in NCC by 0.0146. As the visual quality is highly related to the NCC, more iterations and runtime are expected for SyN to improve the visual performance.

To conclude, the learning-based methods consume much less computation time than the well-known traditional method SyN without compromising the registration accuracy. Experimental results demonstrate that the proposed FDRN provides better Dice score, NCC and visual perception than the existing state-of-the-art approaches for deformable registration of brain MR images. It is necessary to mention that FDRN is a generalized model for deformable image registration and is not limited to brain MR images. It can also be applied to other anatomical structures or CT images such as cardiac MR scans or lung CT images.

Acknowledgements

This work has been funded by the Federal Ministry of Education and Research (BMBF, Germany) under the grand No. 05M18VSA.

References

- ¹ J. A. Maintz and M. A. Viergever, A survey of medical image registration, *Med. Image Anal.* **2**, 1–36 (1998).
- ² J. V. Hajnal, D. L. Hill, and D. J. Hawkes, Medical Image Registration, *Phys. Med. Biol.* **46** (2001).
- ³ B. Fischer and J. Modersitzki, Ill-posed medicine—An introduction to image registration, *Inverse Problems* **24**, 034008 (2008).
- ⁴ A. Sotiras, C. Davatzikos, and N. Paragios, Deformable Medical Image Registration: A Survey, *IEEE Trans. Med. Imag.* **32**, 1153–1190 (2013).

-
- ⁵ M. F. Beg, M. I. Miller, A. Trounev, and L. Younes, Computing large deformation metric mappings via geodesic flows of diffeomorphisms, *Int. J. Comput. Vision* **61**, 139–157 (2005).
- ⁶ P. Viola and W. M. W. III, Alignment by maximization of mutual information, *International journal of computer vision* **24**, 137–154 (1997).
- ⁷ B. B. Avants, C. L. Epstein, M. Grossman, and J. C. Gee, Symmetric diffeomorphic image registration with cross-correlation: Evaluating automated labeling of elderly and neurodegenerative brain, *Med. Image Anal.* **12**, 26–41 (2008).
- ⁸ R. Bajcsy and S. Kovačič, Multiresolution elastic matching, *Comput. Vis., Graph., Image Process.* **46**, 1–21 (1989).
- ⁹ J. C. Gee and R. Bajcsy, Elastic matching: Continuum mechanical and probabilistic analysis, *Brain Warp.* , 183–197 (1999).
- ¹⁰ C. Davatzikos, Spatial transformation and registration of brain images using elastically deformable models, *Comput. Vis. Image Understand* **66**, 207–222 (1997).
- ¹¹ D. Rueckert, L. I. Sonoda, C. Hayes, D. L. G. Hill, M. O. Leach, and D. J. Hawkes, Nonrigid Registration Using Free-Form Deformation: Application to Breast MR Images, *IEEE Trans. Med. Imag.* **18**, 712–721 (1999).
- ¹² J. Kybic and M. Unser, Fast parametric elastic image registration, *IEEE Trans. Image Process.* **12**, 1427–1442 (2003).
- ¹³ J. Kybic and M. Unser, A fast nonrigid image registration with constraints on the Jacobian using large scale constrained optimization, *IEEE Trans. Med. Imag.* **27**, 271–281 (2008).
- ¹⁴ J. Thirion, Image matching as a diffusion process: an analogy with maxwell’s demons, *Med. Image Anal.* **2**, 243–260 (1998).
- ¹⁵ M. F. Beg and A. Khan, Symmetric data attachment terms for large deformation image registration, *IEEE Trans. Med. Imag.* **26**, 1179–1189 (2007).
- ¹⁶ J. Ashburner and K. J. Friston, Diffeomorphic registration using geodesic shooting and Gauss-Newton optimisation, *NeuroImage* **55**, 954–967 (2011).
- ¹⁷ D. Rueckert, A. F. Frangi, and J. A. Schnabel, Automatic construction of 3D statistical deformation models using non-rigid registration, in *International Conference on Medical Image Computing and Computer-Assisted Intervention*, pages 77–84, 2001.
- ¹⁸ D. Rueckert, A. F. Frangi, and J. A. Schnabel, Automatic construction of 3-D statistical deformation models of the brain using nonrigid registration, *IEEE Trans. Med. Imag.* **22**, 1014–1025 (2003).
-

-
- ¹⁹ J. Krebs et al., Robust non-rigid registration through agent-based action learning, in *International Conference on Medical Image Computing and Computer-Assisted Intervention*, pages 344–352, 2017.
- ²⁰ B. Gutiérrez-Becker, D. Mateus, L. Peter, and N. Navab, Learning optimization updates for multimodal registration, in *International Conference on Medical Image Computing and Computer-Assisted Intervention*, pages 19–27, 2016.
- ²¹ B. Gutiérrez-Becker, D. Mateus, L. Peter, and N. Navab, Guiding multimodal registration with learned optimization updates, *Med. Image Anal.* **41**, 2–17 (2017).
- ²² M. Kim, G. Wu, Q. Wang, S. Lee, and D. Shen, Improved image registration by sparse patch-based deformation estimation, *NeuroImage* **105**, 257–268 (2015).
- ²³ Q. Wang, M. Kim, Y. Shi, G. Wu, and D. Shen, Predict brain MR image registration via sparse learning of appearance and transformation, *Med. Image Anal.* **20**, 61–75 (2015).
- ²⁴ J. Fan, X. Cao, P. Yap, and D. Shen, BIRNet: Brain image registration using dual-supervised fully convolutional networks, *Med. Image Anal.* **54**, 193–206 (2019).
- ²⁵ H. Sokooti, B. de Vos, F. Berendsen, B. P. F. Lelieveldt, I. Išgum, and M. Staring, Non-rigid image registration using multi-scale 3D convolutional neural networks, in *International Conference on Medical Image Computing and Computer-Assisted Intervention*, pages 232–239, 2017.
- ²⁶ X. Yang, R. Kwitt, M. Styner, and M. Niethammer, Quicksilver: Fast predictive image registration—a deep learning approach, *NeuroImage* **158**, 378–396 (2017).
- ²⁷ M. M. Rohé, M. Datar, T. Heimann, M. Sermesant, and X. Pennec, SVF-Net: Learning deformable image registration using shape matching, in *International Conference on Medical Image Computing and Computer-Assisted Intervention*, pages 266–274, 2017.
- ²⁸ B. D. deVos, F. F. Berendsen, M. A. Viergever, M. Staring, and I. Išgum, End-to-end unsupervised deformable image registration with a convolutional neural network, in *Deep Learning in Medical Image Analysis and Multimodal Learning for Clinical Decision Support*, pages 204–212, 2017.
- ²⁹ G. Balakrishnan, A. Zhao, M. R. Sabuncu, J. Guttag, and A. V. Dalca, An unsupervised learning model for deformable medical image registration, in *IEEE Conference on Computer Vision and Pattern Recognition*, pages 9252–9260, 2018.
- ³⁰ H. Li and Y. Fan, Non-Rigid Image Registration Using Self-Supervised Fully Convolutional Networks without Training Data, in *IEEE 15th International Symposium on Biomedical Imaging*, pages 1–4, 2018.
- ³¹ M. Jaderberg, K. Simonyan, and A. Zisserman, SVF-Net: Learning deformable image registration using shape matching, in *Advances in Neural Information Processing Systems*, pages 2017–2025, 2015.
-

-
- ³² O. Ronneberger, P. Fischer, and T. Brox, U-net: Convolutional networks for biomedical image segmentation, in *International Conference on Medical image computing and computer-assisted intervention*, pages 234–241, Springer, 2015.
- ³³ G. Balakrishnan, A. Zhao, M. R. Sabuncu, J. Guttag, and A. V. Dalca, Voxelmorph: a learning framework for deformable medical image registration, *IEEE Trans. Med. Imag.* **38**, 1788–1800 (2019).
- ³⁴ D. W. Shattuck et al., Construction of a 3D probabilistic atlas of human cortical structures, *Neuroimage* **39**, 1064–1080 (2008).
- ³⁵ A. D. Martino et al., The autism brain imaging data exchange: towards a large-scale evaluation of the intrinsic brain architecture in autism, *Molecular psychiatry* **19**, 659–667 (2014).
- ³⁶ S. G. Mueller et al., Ways toward an early diagnosis in Alzheimer’s disease: the Alzheimer’s Disease Neuroimaging Initiative (ADNI), *Alzheimer’s & Dementia* **1**, 55–66 (2005).
- ³⁷ V. Fonov et al., Unbiased average age-appropriate atlases for pediatric studies, *Neuroimage* **54**, 313–327 (2011).
- ³⁸ L. R. Dice, Measures of the amount of ecologic association between species, *Ecology* **26**, 297–302 (1945).
- ³⁹ Z. Wang, A. C. Bovik, H. R. Sheikh, and E. P. Simoncelli, Image quality assessment: from error visibility to structural similarity, *IEEE Trans. Image Process.* **13**, 600–612 (2004).
- ⁴⁰ B. B. Avants, N. J. Tustison, G. Song, P. A. Cook, A. Klein, and J. C. Gee, A reproducible evaluation of ANTs similarity metric performance in brain image registration, *Neuroimage* **54**, 2033–2044 (2011).